arXiv:1408.3737v1 [math.NA] 16 Aug 2014

NUMERICAL SIMULATION OF FLUID-STRUCTURE INTERACTION PROBLEMS WITH HYPERELASTIC MODELS: A MONOLITHIC APPROACH

ULRICH LANGER AND HUIDONG YANG

Abstract. In this paper, we consider a monolithic approach to handle coupled fluid-structure interaction problems with different hyperelastic models in an all-at-once manner. We apply Newtons method in the outer iteration dealing with nonlinearities of the coupled system. We discuss preconditioned Krylov sub-space, algebraic multigrid and algebraic multilevel methods for solving the linearized algebraic equations. Finally, we compare the results of the monolithic approach with those of the corresponding partitioned approach that was studied in our previous work.

1. Introduction

Parallel to the development of the partitioned approach for the fluid-structure interaction (FSI) simulation (see, e.g., [24, 8, 51, 38, 29]), the monolithic one also attracts many interests in the last decade; see, e.g., [11, 23, 9, 34, 14, 40, 61, 12]. Compare to the flexibility of the partitioned approach, where existing fluid and structure sub-problem solvers can be directly reused or adapted in an iterative manner, the monolithic one behaves more stable and robust by dealing with the coupled nonlinear FSI system in an all-at-once manner. Formally speaking, we apply Newton's method (see [26]) in an outer iteration dealing with nonlinearities originated from the domain movements, convection terms, material laws, transmission conditions and stabilization parameters (that may depend on the solution itself); as a price to pay, at each Newton iteration, a large linearized system is to be solved efficiently.

In the monolithic approach, the linearization of the nonlinear coupled system turns out to be a nontrivial task and requires tedious work on both the analytical derivation and computer implementation. One difficulty considered in this work results from the hyperelastic nonlinear material law as for the thick-walled artery with the media and adventitia layer (see [42, 33]), for which the second and fourth order tensors of the energy functional with respect to the right Cauchy-Green tensor demand heavy amount of computational effort in each Newton iteration;

see, e.g., [41, 16] for an introduction on the basic tools used to derive these quantities under the Lagrangian framework and e.g., [4] for the simulation of such arterial tissues. Thanks to our previous work in [52], the linearization for the hyperelastic models tackled in a partitioned FSI solver is reused in this work. Another difficulty stems from the fluid domain movement handled by the Arbitrary-Lagrangian-Eulerian (ALE) method, where the fluid domain displacement is introduced as an additional variable; see, e.g., [45, 30, 27]. To formalize the derivative of the fluid sub-problem with respect to the fluid domain displacement, the domain mapping (see, e.g., [75]) and shape derivative calculus (see, e.g., [14, 2]) are two typical robust approaches mainly considered so far. In the domain mapping approach, the fluid sub-problem is mapped to the one on the reference (initial) fluid domain via the ALE mapping, that matches the Lagrangian structure domain on the interface for all the time. Therefore, the FSI transmission conditions are defined on the unchanged interface between the fluid and structure reference domains. By transforming the fluid sub-problem from the current domain (ALE framework) to the reference domain (Lagrangian framework), the fluid domain deformation gradient tensor and its determinant arise, which leads to a formulation similar to the one under the Lagrangian framework as usually adopted in continuum mechanics. Thus, for the fluid sub-problem, we follow the same approach to compute the directional derivative with respect to the fluid domain displacement (see related techniques in, e.g., [41, 16]) as we used for the hyperelastic equations in [52]. In the second approach based on a shape derivative technique (see, e.g., [67]), the derivative of the fluid sub-problem is then evaluated by computing the directional derivative with respect to the change of geometry (a small perturbation) on the current domain; see also this technique employed by the partitioned Newton's method in [24, 79].

In addition to the effort on the linearization of the coupled nonlinear system, the monolithic solver requires the properly designed preconditioners and solvers (as inner iteration) for the linearized coupled FSI system at each Newton iteration and may demand more effort. In [61], the preconditioned Krylov subspace method (see, e.g., [63]) and geometrical multigrid method (see, e.g., [39]) with a Vanka-like smoother are employed to solve the linearized and discretized 2D FSI system using the high order $Q_2 - P_1$ stabilized finite element pair. For the complex 3D geometries and unstructured meshes, in [34], the GMRES method (see [64]) accelerated by the block Gauss-Seidel preconditioner is considered, for which the block inverse is approximated by smoothed aggregation multigrid (see, e.g., [65]) for each sub-problem. In order to improve the performance, a monolithic FSI algebraic multigrid

(AMG) method using preconditioned Richardson iterations with potentially level-dependent damping parameters as smoothing steps is further developed therein. Besides, the monolithic solver is shown capable of utilizing parallel computing resources. In [23], parallel preconditioners of the coupled problem based on the algebraic additive Schwarz (see, e.g., [70]) preconditioners for the sub-problems are built for both the convective explicit and geometry-convective explicit time discretized FSI systems. As a 2D counterpart, in [11], a one-level additive Schwarz preconditioner (see, e.g., [70]) for the linearized system is considered for the fully implicit time discretized FSI system, that is based on a sub-domain preconditioner constructed on an extention of a non-overlapping sub-domain to its neighbors.

In this work, we focus on the development and comparison of different monolithic solution methods, namely, the Krylov subspace methods preconditioned by the block LU decomposition of the coupled system, the AMG and algebraic multilevel (AMLI [5, 7, 72, 6, 50, 49], also referred to as K-cycle [57, 59]) method, applied to the coupled FSI system with nearly incompressible hyperelastic models (see [42, 33]). Our solution methods are mainly based on a class of special AMG methods developed in [47] and [73, 74], for the discrete elliptic and saddle point problems, respectively, where the robust matrix-graph based coarsening strategies are proposed in a (pure) algebraic manner. This class of AMG methods have been applied to the sub-problems in the fluid-structure interaction simulation; see [79, 78, 77, 52]. Particularly in our recent work [52], we have developed this approach by carefully choosing the effective smoothers: Braess-Sarazin smoother (see [17, 80]) and Vanka smoother (see [71, 76]), for the linearized Navier-Stokes equations under the ALE framework and hyperelastic equations under the Lagrangian framework, respectively. In order to further extend this class of AMG methods to the monolithic coupled FSI system after linearization, the two essential components in the AMG methods, the coarsening strategy and the smoother, for the coupled system are to be developed. Namely, the robust coarsening strategy using the stabilized Galerkin projection is constructured based on the $\inf - \sup$ condition (see, e.g., [18, 35]) on coarse levels for the indefinite sub-problems. By this means, we obtain the stabilized coupled systems on coarse levels. The effective smoother is designed by damped block Gauss-Seidel iterations applied to the coupled system, that are based on the AMG cycles for the mesh movement, fluid and structure sub-problem, respectively. According to our numerical experiments, we observe the robustness of the damping parameter with respect to the AMG levels and different hyperelastic models adopted in the FSI simulation. As

a variant of our coupled AMG method, we further consider the AMLI method for the coupled FSI system, in which we use the hierarchy of the coupled systems constructured in an algebraic manner as in the AMG methods. The smoothing for the coarse grid correction equation is performed by a flexible GMRES (FGMRES [62]) scheme preconditioned by the multilevel preconditioner; see, e.g., [3] the application for the non-regularized Bingham fluid problem using the geometric multigrid method. In order to improve the performance, we finally consider the GMRES and FGMRES Kyrlov sub-space method preconditioned with such AMG and AMLI cycles.

The remainder of the paper is organized in the following way. In Section 2, the coupled FSI system using a family of hyperelastic models for a model problem is formulated in a monolithic way. Section 3 deals with the temporal and spatial discretization, and Newton's method tackling the linearization for the coupled nonlinear FSI system. In Section 4, several monolithic solution methods for the linearized FSI system are considered in detail. Some numerical experiments are presented in Section 5. Finally, in Section 6, some conclusions are drawn.

2. A model problem

2.1. **Computational domains and mappings.** We consider a model problem in the computational FSI domain Ω^t at time t decomposed into the fluid domain Ω_f^t and the structure domain Ω_s^t, i.e., $\overline{\Omega^t} = \overline{\Omega_f^t} \cup \overline{\Omega_s^t}$ and $\Omega_f^t \cap \Omega_s^t = \emptyset$. Let Γ_d^0 and Γ_n^0 denote the boundaries with the homogeneous Dirichlet and Neumman condition for the structure sub-problem, respectively, Γ_{in}^t and Γ_{out}^t the boundaries with the inflow and outflow condition for the fluid sub-problem, respectively, $\Gamma_f^0 = \overline{\Gamma_d^0} \cap (\overline{\Gamma_{in}^0} \cup \overline{\Gamma_{out}^0})$ the fluid boundary with the homogeneous velocity condition, Γ^t the interface between two domains: $\Gamma^t = \partial\Omega_f^t \cap \partial\Omega_s^t \setminus \Gamma_f^0$. At time $t = 0$, we have all the initial configurations. See an illustration in Fig. 1.

As usually adopted, we use the Lagrangian mapping (see, e.g., [41, 16, 60]) $\mathcal{L}^t(\cdot) : \mathcal{L}^t(x_0) = x_0 + d_s(x_0, t)$ for all $x_0 \in \Omega_s^0$ and $t \in (0, T)$ to track the motion of the structure body, where $d_s(\cdot, \cdot)$ denotes the structure displacement, i.e., $d_s(\cdot, \cdot) : \Omega_s^0 \times (0, T] \mapsto \mathbb{R}^3$. For the fluid sub-problem, we employ the arbitrary Lagrangian Eulerian (ALE, see, e.g., [45, 27, 30]) mapping $\mathcal{A}^t(\cdot)$ on Ω_f^0 to track the fluid domain monition, i.e., $\mathcal{A}^t(x_0) = x_0 + d_f(x_0, t)$ for all $x_0 \in \Omega_f^0$ and $t \in (0, T)$, where the fluid displacement $d_f(\cdot, \cdot) : \Omega_f^0 \times (0, T] \mapsto \mathbb{R}^3$ follows the fluid and structure particle motion on the Γ^0, and is arbitrary extended into the fluid domain Ω_f^0 (see, e.g., [75]). The fluid domain velocity $w_f(\cdot, \cdot) : \Omega_f^0 \times (0, T] \mapsto \mathbb{R}^3$ is then given by $w_f = \partial_t d_f$. With help of

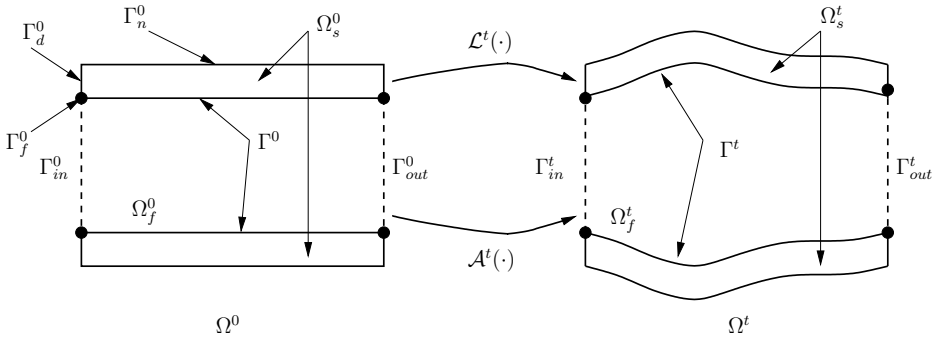

FIGURE 1. A schematic illustration of the domain mappings.

this mapping, the fluid velocity $u(\cdot,\cdot) : \Omega_f^0 \times (0,T] \mapsto \mathbb{R}^3$ and pressure $p(\cdot,\cdot) : \Omega_f^0 \times (0,T] \mapsto \mathbb{R}$ are defined by the transformation:

$$u(x,t) = \tilde{u}(\tilde{x},t) = \tilde{u}(\mathcal{A}_f^t(x),t), \tag{1a}$$

$$p(x,t) = \tilde{p}(\tilde{x},t) = \tilde{p}(\mathcal{A}_f^t(x),t), \tag{1b}$$

for all $x \in \Omega_f^0$ and $\tilde{x} = \mathcal{A}_f^t(x) \in \Omega_f^t$. Here for simplicity of notations, $\tilde{u}(\cdot,\cdot)$ and $\tilde{p}(\cdot,\cdot)$ are used to indicate the variables under the Eulerian framework.

2.2. **Basic notations in Kinematics.** In order to formulate the coupled system on the reference domain Ω^0, we first introduce the following basic notations in Kinematics of nonlinear continuum mechanics; see, e.g., [41, 16, 60]. Let $F_f = \partial\mathcal{A}^t/\partial x = I + \nabla d_f$ for $x \in \Omega_f^0$ and $F_s = \partial\mathcal{L}^t/\partial x = I + \nabla d_s$ for $x \in \Omega_s^0$ denote the fluid and structure deformation gradient tensor, respectively. The determinant is given by $J_f = \det F_f$ and $J_s = \det F_s$, respectively. For the nonlinear hyperelastic models, further notations are used, namely, the right Cauchy-Green tensor $C = F_s^T F_s$ and the three principal invariants $I_1 = C : I$, $I_2 = 0.5(I_1^2 - C : C)$ and $I_3 = \det C$, respectively. Furthermore, the second Piola-Kirchoff tensor S is defined by $S = 2\partial\Psi/\partial C$, where Ψ denotes the invariant dependent energy functional determined by the material properties.

2.3. **A family of hyperelastic models.** A family of hyperleastic models are used in this work, that posses nearly incompressible or anisotropic properties; see, e.g., [16, 41, 42, 33, 4]. We first consider the model of Neo-Hookean material, for which the energy functional is given by

$$\Psi = 0.5c_{10}(J_1 - 3) + 0.5\kappa(J_s - 1)^2, \tag{2}$$

where $J_1 = I_1 I_3^{-1/3}$ denotes the invariant, κ the bulk modulus and c_{10} the material parameter related to the shear modulus. The second Piolad-Kirchoff tensor is then given by

$$S = S^{'} - p_s J_s C^{-1} \tag{3}$$

with $S^{'} = c_{10}\partial J_1/\partial C$, where the structure pressure $p_s := p_s(x,t) = -\kappa(J_s - 1) : \Omega_s^0 \times (0,T] \mapsto \mathbb{R}^3$ is introduced in order to overcome the locking phenomena with large bulk modulus; see, e.g., [48, 53, 36, 69].

We then consider the modified model of Mooney-Rivlin material, for which the energy functional is given by

$$\Psi = 0.5c_{10}(J_1 - 3) + 0.5c_{01}(J_2 - 3) + 0.5\kappa(J_s - 1)^2, \tag{4}$$

where $J_2 = I_2 I_3^{-2/3}$ denotes the invariant and c_{01} the material parameter related to the shear modulus. The second Piolad-Kirchoff tensor is then accordingly given by

$$S = S^{'} - p_s J_s C^{-1}, \tag{5}$$

where $S^{'} = c_{10}\partial J_1/\partial C + c_{01}\partial J_2/\partial C$.

We finally consider the model of the anisotropic two-layer thick-walled artery; see [42, 33]. The energy functional of such an arterial model is defined by

$$\Psi = 0.5c_{10}(J_1 - 3) + \Psi_{\text{aniso}} + 0.5\kappa(J_s - 1)^2 \tag{6}$$

with $\Psi_{\text{aniso}} = 0.5k_1k_2\sum_{i=4,6}(\exp(k_2(J_i-1)^2)-1)$, where k_1 and k_2 are a stress-like material parameter and a dimensionless parameter, respectively, associated with contribution of collagen to the response, and $J_4 > 1$ and $J_6 > 1$ are invariants active in extension, that are defined as $J_4 = I_3^{-1/3}A_1 : C$ and $J_6 = I_3^{-1/3}A_2 : C$, respectively. The tensors $A_1 = a_{01} \otimes a_{01}$ and $A_2 = a_{02} \otimes a_{02}$ are prescribed with the direction vectors $a_{01} = (0, \cos\alpha, \sin\alpha)^T$ and $a_{02} = (0, \cos\alpha, -\sin\alpha)^T$, respectively, where $\alpha \in \{\alpha_M, \alpha_A\}$ denotes the angle between the collagen fibers and the circumferential direction in the media and adventitia, respectively. The second Piola-Kirchoff tensor S for this hyperelastic model is computed as

$$S = S^{'} - p_s J_s C^{-1} \tag{7}$$

with $S^{'} = c_{10}\partial J_1/\partial C + k_1\sum_{i=4,6}(\exp(k_2(J_i - 1)^2(J_i - 1))\partial J_i/\partial C)$. In our numerical experiments, we use the geometrical configuration and material parameters of a rabbit carotid artery prescribed in [42]. For

modeling arterials in the FSI simulation considering specific fiber orientation, prestress and zero-stress configurations, and viscoelastic support conditions, we further refer to [14, 68, 43, 56, 55, 15, 13] for relevant details.

2.4. **Coupled fluid-structure interaction system.** The coupled FSI system in strong form reads: Find (d_f, u, p_f, d_s, p_s) such that

$$-\Delta d_f = 0 \quad \text{in } \Omega_f^0, \tag{8a}$$

$$d_f = d_s \quad \text{on } \Gamma^0, \tag{8b}$$

$$\begin{aligned} \rho_f J_f \partial_t u + \rho_f J_f((u - w_f) \cdot F_f^{-1}\nabla)u \\ -\nabla \cdot (J_f \sigma_f(u, p_f) F_f^{-T}) = 0 \quad \text{in } \Omega_f^0, \end{aligned} \tag{8c}$$

$$\nabla \cdot (J_f F_f^{-1} u) = 0 \quad \text{in } \Omega_f^0, \tag{8d}$$

$$\rho_s \partial_{tt} d_s - \nabla \cdot (F_s S) = 0 \quad \text{in } \Omega_s^0, \tag{8e}$$

$$-(J_s - 1) - (1/\kappa) p_s = 0 \quad \text{in } \Omega_s^0, \tag{8f}$$

$$u = \partial_t d_s \quad \text{on } \Gamma^0, \tag{8g}$$

$$J_f \sigma_f(u, p_f) F_f^{-T} n_f + F_s S n_s = 0 \quad \text{on } \Gamma^0, \tag{8h}$$

supplemented with the corresponding boundary conditions $d_f = 0$ on $\Gamma_{in}^0 \cup \Gamma_{out}^0$, $u = 0$ on Γ_f^0, $J_f \sigma_f(u, p_f) F_f^{-T} n_f = g_{in}$ (a given function) on Γ_{in}^t and $J_F \sigma_f(u, p_f) F_f^{-T} n_f = 0$ on Γ_{out}^t, $d_s = 0$ on Γ_d^0 and $F_s S n_s = 0$ on Γ_n^0, and proper initial conditions $u(x, 0) = 0$ for all $x \in \Omega_f^0$ and $d_s(x, 0) = \partial_t d_s(x, 0) = 0$ for all $x \in \Omega_s^0$. Here ρ_f and ρ_s denote the fluid and structure density, respectively, n_f and n_s the fluid and structure outerward unit normal vector, respectively, $\sigma_f(u, p_f) := \mu(\nabla u + \nabla^T) - p_f I$ the Cauchy stress tensor with the dynamic viscosity term μ. Note that for the fluid sub-problem, we transform the momentum balance and mass conservation equations from the Eulerian to Lagrangian framework using the ALE mapping.

3. Temporal and spatial discretization and linearization

3.1. **The temporal discretization.** For the time discretization of the fluid sub-problem, we use the first order implicit Euler scheme. Let $u^n := u(\cdot, t^n)$ and $w^n := w(\cdot, t^n) = \partial_t d_f(\cdot, t^n)$ denote the approximateions of the fluid and fluid domain velocity at time level $t^n = n\Delta t$, $n = 1, ..., N$, $\Delta t = T/N$, i.e., the time period $(0, T]$ is subdivided into N equidistant intervals. At time level t^0, the FSI solution is given by the initial conditions. The time derivatives at the level t^n are then

approximated as

$$\partial_t u^n \approx (u^n - u^{n-1})/\Delta t, \tag{9a}$$
$$w^n \approx (d^n - d^{n-1})/\Delta t. \tag{9b}$$

For the structure sub-problem, a first order Newmark-β scheme is used (see [58]), i.e.,

$$\ddot{d}_s^n \approx \frac{1}{\beta\Delta t^2}(d_s^n - d_s^{n-1}) - \frac{1}{\beta\Delta t}\dot{d}_s^{n-1} - (\frac{0.5}{\beta} - 1)\ddot{d}_s^{n-1}, \tag{10a}$$
$$\dot{d}_s^n \approx \dot{d}_s^{n-1} + \gamma\Delta t\ddot{d}_s^n + (1-\gamma)\Delta\ddot{d}_s^{n-1}, \tag{10b}$$

where $0 < \beta \leq 1$ and $0 \leq \gamma \leq 1$.

3.2. **The time semi-discretized weak formulation.** In order to find the finite element FSI solution on proper function spaces, we first formulate the weak formulation for the coupled system (8). We introduce the notations $H^1(\Omega_f^0)$, $H^1(\Omega_s^0)$ and $L^2(\Omega_f^0)$ for the standard Sobolev and Lebesgue spaces (see, e.g., [1]) on Ω_f^0 and Ω_s^0, respectively. Let $V_m := H^1(\Omega_f^0)^3$ be the fluid domain displacement space, $V_f := H^1(\Omega_f^0)^3$ and $Q_f := L^2(\Omega_f^0)$ be the fluid velocity and pressure space, respectively. The function spaces V_s and Q_s for the structure displacement and pressure shall be properly chosen regarding the nonlinearities; see, e.g., [10, 22]. Incorporating boundary conditions, we further introduce the following function space notations: $V_{m,D}^n := \{v \in V_m : v = d_s^n \text{ on } \Gamma^0\}$, $V_{m,0} := \{v \in V_m : v = 0 \text{ on } \Gamma_{in}^0 \cup \Gamma_{out}^0\}$ for the mesh movement sub-problem, $V_{f,0} := \{v \in V_f : v = 0 \text{ on } \Gamma_f^0\}$ for the fluid sub-problem, $V_{s,D}^n := \{v \in V_s : v = 0 \text{ on } \Gamma_d^0 \mid v = u^n\Delta t + v^{n-1} \text{ on } \Gamma^0\}$, $V_{s,0} := \{v \in V_s : v = 0 \text{ on } \Gamma_d^0 \cup \Gamma^0\}$ for the structure sub-problem.

The weak formulation for the coupled system (8) reads: Find $(d_f^n, u_f^n, p_f^n, d_s^n, p_s^n) \in (V_{m,D}, V_{f,0}, Q_f, V_{s,D}^n, Q_s)$ such that for all $(v_m, v_f, q_f,$

$v_s,\, q_s) \in (V_{m,0},\, V_{f,0},\, Q_f,\, V_{s,0},\, Q_s)$

$$(\nabla d_f^n, \nabla v_m)_{\Omega_f^0} = 0 \quad , \tag{11a}$$

$$\begin{aligned} &\rho_f(J_f(u^n - u^{n-1})/\Delta t, v_f)_{\Omega_f^0} \\ &+\rho_f(J_f((u^n - (d_f^n - d_f^{n-1})/\Delta t) \cdot F_f^{-1}\nabla)u^n, v_f)_{\Omega_f^0} \\ &-\langle g_{in}, v_f\rangle_{\Gamma_{in}^0} + (J_f\sigma_f(u^n, p_f^n)F_f^{-T}, \nabla v_f)_{\Omega_f^0} = 0 \quad , \end{aligned} \tag{11b}$$

$$-(\nabla \cdot (J_f F_f^{-1} u^n), v_f)_{\Omega_f^0} = 0 \quad , \tag{11c}$$

$$\begin{aligned} &(\beta_2 d_s^n, v_s)_{\Omega_s^0} + (S^{'}, F_s^T \nabla v_s)_{\Omega_s^0} \\ &-(J_s - 1, q_s)_{\Omega_s^0} - (1/\kappa)(p_s^n, q_s)_{\Omega_s^0} = 0 \quad , \end{aligned} \tag{11d}$$

$$-(p_s J_s F_s^{-T}, \nabla v_s)_{\Omega_s^0} = 0 \quad , \tag{11e}$$

$$\langle J_f\sigma_f(u^n, p_f^n)F^{-T}n_f, v_f\rangle_{\Gamma^0} + \langle F_s S n_s, v_s\rangle_{\Gamma^0} = 0 \quad , \tag{11f}$$

with $r_s = \beta_2 d_s^{n-1} + \beta_1 \dot{d}_s^{n-1} + \rho_s(0.5/\beta - 1)\ddot{d}_s^{n-1}$, where $\beta_2 = \rho_s/(\beta\Delta t^2)$ and $\beta_1 = \rho_s/(\beta\Delta t)$. As observed, the fluid sub-problem is coupled with the mesh movement sub-problem in Ω_f^0 and coupled with the structure sub-problem on Γ^0. The mesh movement sub-problem is coupled with the structure sub-problem on Γ^0. The equilibrium of surface tractions on Γ^0 is realized by the equilibrium of the residual of the weak formulation for the fluid and structure momentum equations with non-vanishing test functions $v_f \in V_{f,0}$ and $v_s \in V_{s,0}$ on Γ^0, where $v_f = v_s$ on Γ^0; see [79].

3.3. **The spatial discretization and stabilization.** As in [52], we use Netgen [66] to generate the tetrahedral mesh of the computational FSI domain Ω^0 with conforming grids on the FSI interface and resolved different structure layers. For the mesh movement, we use P_1 finite element on the tetrahedral mesh. For the fluid and structure sub-problem, we use $P_1 - P_1$ finite element with stabilization in order to fulfill the inf $-$ sup or LBB (Ladyshenkaya-Babuška-Brezzi) stability condition (see, e.g., [18, 35]), and to tackle the instability in advection dominated regions of the domain. In particular, we employ a unified streamline-upwind and pressure-stabilizing Petrov-Galerkin (SUPG/PSPG) method (see, e.g., [44, 19, 25, 32, 31]) to stabilize the $P_1 - P_1$ discretized fluid sub-problem. For the structure sub-problem, we use the PSPG method (see, e.g., [44, 48, 53, 36]) to suppress the instability caused by equal order finite element interpolation spaces for the displacement and pressure. The application of this stabilization technique to the hyperelastic equations of anisotropic two-layer thick walled artery is prescribed in [52].

3.4. **Newton's method for the nonlinear FSI system.** Formally speaking, after discretization in time and space of the coupled FSI system (8), we obtain the following nonlinear finite element algebraic equation

$$\mathcal{R}(X) = 0 \tag{12}$$

with

$$\mathcal{R}(\cdot) = \begin{bmatrix} R_{ms}(\cdot) \\ R_{mfs}(\cdot) \\ R_{sf}(\cdot) \end{bmatrix} \text{ and } X = \begin{bmatrix} D_m \\ U_f \\ U_s \end{bmatrix}, \tag{13}$$

where the subscripts m, f and s representing mesh movement, fluid and structure, respectively, and ms, mfs and sf the coupling among corresponding sub-problems. Furthermore $R_{ms}(X) = 0$, $R_{mfs}(X) = 0$ and $R_{sf}(X) = 0$ stand for the finite element equations for the fluid mesh movement sub-problem coupled with the Dirichlet boundary condition on Γ^0 from the structure sub-problem, for the fluid sub-problem coupled with the fluid domain displacement from the mesh movement sub-problem and Neumann boundary condition on Γ^0 from the structure sub-problem, for the structure sub-problem coupled with the Dirichlet boundary condition on Γ^0 from the fluid sub-problem, respectively. The finite element solutions of the fluid domain displacement, fluid velocity and pressure, and structure displacement and pressure are denoted by D_m, U_f and U_s, respectively.

Newton's method applied to the nonlinear coupled FSI equation (12) is presented in Algorithm 1, where $\mathcal{J}_k$ denote the Jacobian matrix and δx_k the corrections of the finite element solutions at the kth step nonlinear iteration. Note that the two terms $\partial R_{ms}/\partial U_s$ and $\partial R_{sf}/\partial U_f$ take the derivatives with respect to the structure displacement and fluid velocity, respectively, that corresponds to the linearization of two Dirichlet interface conditions on Γ^0 between the fluid and structure domain displacement, and between the fluid and structure velocity, respectively. The linearization of the Neumann interface condition on Γ^0 and of the fluid sub-problem are given in the second row of $\mathcal{J}_k$. The linearization of structure sub-problem is given in the third row of $\mathcal{J}_k$.

Besides the costly assembly procedure of $\mathcal{J}_k$ in (14), another main cost in Algorithm 1 is to solve the linearized equation (15). More precisely, we come up with the linearized FSI system in the following reordered form (17) that we aim to solve (for simplicity of notations,

Algorithm 1 Newton's method

Given initial X_0, for $k \geq 0$,

1: assemble the Jacobian matrix $\mathcal{J}_k$ at the current state X_k: for (12)

$$\mathcal{J}_k = \mathcal{R}'(X_k) = \begin{bmatrix} \frac{\partial R_{ms}}{\partial D_m} & 0 & \frac{\partial R_{ms}}{\partial U_s} \\ \frac{\partial R_{mfs}}{\partial D_m} & \frac{\partial R_{mfs}}{\partial U_f} & \frac{\partial R_{mfs}}{\partial U_s} \\ 0 & \frac{\partial R_{sf}}{\partial U_f} & \frac{\partial R_{sf}}{\partial U_s} \end{bmatrix} \begin{pmatrix} D_{m,k} \\ U_{f,k} \\ U_{s,k} \end{pmatrix}, \tag{14}$$

2: solve the linearize system up to a relative residual error reduction factor ε_l:

$$\mathcal{J}_k \delta x_k = -\mathcal{R}(X_k), \tag{15}$$

3: update the solution $X_{k+1} = X_k + \delta x_k$, and go to step 1, until the relative residual error reduction with the factor ε_n is fulfilled:

$$\|X_{k+1} - X_k\|_{L_2} \leq \varepsilon_n \|X_1 - X_0\|_{L_2}. \tag{16}$$

we neglect the subscript k and zero matrix entries):

(17)

$$\begin{bmatrix} A_m^{ii} & A_m^{i\gamma} & & & & & & \\ & I & & & & -I & & \\ B_{fm}^i & B_{fm}^\gamma & -C_f & B_{1f}^i & B_{1f}^\gamma & & & \\ A_{fm}^{ii} & A_{fm}^{i\gamma} & B_{2f}^i & A_f^{ii} & A_f^{i\gamma} & & & \\ A_{fm}^{\gamma i} & A_{fm}^{\gamma\gamma} & B_{2f}^\gamma & A_f^{\gamma i} & A_f^{\gamma\gamma} & A_s^{\gamma\gamma} & A_s^{\gamma i} & B_{2s}^\gamma \\ & & & & -I & \frac{1}{\Delta t} I & & \\ & & & & & A_s^{i\gamma} & A_s^{ii} & B_{2s}^i \\ & & & & & B_{1s}^\gamma & B_{1s}^i & -C_s \end{bmatrix} \begin{bmatrix} \Delta d_m^i \\ \Delta d_m^\gamma \\ \Delta p_f \\ \Delta u_f^i \\ \Delta u_f^\gamma \\ \Delta d_s^\gamma \\ \Delta d_s^i \\ \Delta p_s \end{bmatrix} = \begin{bmatrix} r_m^i \\ r_m^\gamma \\ r_{p_f} \\ r_f^i \\ r_f^\gamma \\ r_s^\gamma \\ r_s^i \\ r_{p_s} \end{bmatrix},$$

where the superscripts γ and i are used to denote qualities associated to the nodal degrees of freedom (DOF) on the interface and the total remaining DOF in the domain and on the other boundaries of the domain. Furthermore, the qualities with the superscripts $\gamma\gamma$, ii, γi and $i\gamma$ indicate, that they result from the coupling of corresponding DOF. The solution posses a symbol Δ in front, indicating the DOF of the correction. It is easy to see from (17) how the sub-problems are linearized and coupled in a big FSI system. On the computer implementation, we are not explictly assembling the system (17), but the separate system for each sub-problem. The matching conditions are imposed implicitly by the conforming grids on the interface. This is easily implemented in the preconditioned Krylov subspace methods.

The monolithic algebraic multigrid and multilevel approaches for the big coupled system require the formal systems on coarse levels. Furthermore, a direct solver is usually applied on the coarsest level, which requires an explictly formed system. Therefore, it is convenient and practical to form the big system in an explicit way and meanwhile to keep the flexibility of system assembling for each sub-problem. Therefore, we reformulate the system (17) as

$$Kx = b \tag{18}$$

with

$$K = \begin{bmatrix} A_m & 0 & A_{ms} \\ A_{fm} & A_f & A_{fs} \\ 0 & A_{sf} & A_s \end{bmatrix}, x = \begin{bmatrix} \Delta d_m \\ \Delta u_f \\ \Delta u_s \end{bmatrix}, b = \begin{bmatrix} r_m \\ r_f \\ r_s \end{bmatrix}, \tag{19}$$

where A_m, A_f and A_s represent the mesh movement, fluid and structure stiffness matrix from the finite element assembly, respectively , which are permuted from the corresponding ones in (17) according to their local nodal numbering of the finite element mesh for each sub-problem. The coupling matrix between $i \in \{m, f, s\}$ and $j \in \{m, f, s\}$ are denoted by A_{ij}, $i \neq j$. The solution vectors Δd_m, Δu_f and Δu_s denote the DOF of the correction for the fluid domain displacement, fluid velocity and pressure, and structure displacement and pressure, respectively. The residual vectors are presented by r_m, r_f and r_s for the fluid domain movement, fluid and structure sub-problem, respectively. These qualities are similar to the ones in (17), except that they are not recorded based on the separation of the interface and remaing DOF. For consistency of notations, we will restrict our discussion to the solution methods of the linearized system (18) from now on.

4. Monolithic solution methods for the coupled system

In this section, we discuss and compare different monolithic solution methods, namely, the preconditioned Krylov subspace methods, the algebraic multigrid and algebraic multilevel method, applied to the coupled system (18).

4.1. **The preconditioned Krylov subspace methods.**

Because of the block structure of the system matrix K in (18), we discuss some preconditioners mainly based on the LU decomposition (see, e.g., [63]). The inverse of the preconditioner applied to a given vector is easily realized using our efficient AMG methods for sub-problems (see [52]).

4.1.1. *The block-diagonal preconditioner.* We first consider the simplest block-diagonal preconditioner $\tilde{P}_D$, that is obtained by approximating

$$P_D = \begin{bmatrix} A_m & & \\ & A_f & \\ & & A_s \end{bmatrix} \text{ with } \tilde{P}_D = \begin{bmatrix} \tilde{A}_m & & \\ & \tilde{A}_f & \\ & & \tilde{A}_s \end{bmatrix}, \tag{20}$$

where $\tilde{A}_i = A_i(I - M_i^j)^{-1}$, $i \in \{m, f, s\}$, are corresponding multigrid preconditioners for each sub-problem; see, e.g, [37, 46]. The inverse of $\tilde{P}_D$ is easily evaluated by

$$\tilde{P}_D^{-1} = \begin{bmatrix} \tilde{A}_m^{-1} & & \\ & \tilde{A}_f^{-1} & \\ & & \tilde{A}_s^{-1} \end{bmatrix}, \tag{21}$$

which corresponds to one AMG iteration applied to each sub-problem, that is developed in [52]. This preconditioner completely neglects the coupling conditions among different sub-problems.

4.1.2. *The block lower triangular preconditioner.* The block lower triangular preconditioner $\tilde{P}_L$ is obtained by approximating

$$P_L = \begin{bmatrix} A_m & & \\ A_{fm} & A_f & \\ 0 & A_{sf} & A_s \end{bmatrix} \text{ with } \tilde{P}_L = \begin{bmatrix} \tilde{A}_m & & \\ A_{fm} & \tilde{A}_f & \\ 0 & A_{sf} & \tilde{A}_s \end{bmatrix}. \tag{22}$$

It is easy to see the inverse of $\tilde{P}_L$ is given by

$$\tilde{P}_L^{-1} = \begin{bmatrix} \tilde{A}_m^{-1} & & \\ -\tilde{A}_f^{-1}A_{fm}\tilde{A}_m^{-1} & \tilde{A}_f^{-1} & \\ -\tilde{A}_s^{-1}A_{sf}\tilde{A}_f^{-1}A_{fm}\tilde{A}_m^{-1} & -\tilde{A}_s^{-1}A_{sf}\tilde{A}_f^{-1} & \tilde{A}_s^{-1} \end{bmatrix}, \tag{23}$$

which is nothing but a block Gauss-Seidel iteration (using forward substitution) with zero initial guess applied to (18). This is easily computed since we have efficient AMG methods to approximate the inverse of A_m, A_f and A_s. It is also easy to see one inverse operation of $\tilde{P}_L$ only requires (approximately) inverting A_m, A_f and A_s once. This preconditioner has taken into account the coupling block A_{fm}, the directional derivative of the fluid sub-problem with respect to the fluid domain displacement.

4.1.3. *The block upper triangular preconditioner.* We then consider the block upper triangular preconditioner $\tilde{P}_U$ obtained by approximating

$$P_U = \begin{bmatrix} A_m & 0 & A_{ms} \\ & A_f & A_{fs} \\ & & A_s \end{bmatrix} \text{ with } \tilde{P}_U = \begin{bmatrix} \tilde{A}_m & 0 & A_{ms} \\ & \tilde{A}_f & A_{fs} \\ & & \tilde{A}_s \end{bmatrix}. \tag{24}$$

The coupling blocks A_{ms} and A_{fs} are included, which represent the coupling of the Dirichlet interface condition between the fluid and structure domain displacement, and the coupling of the Neumann interface condition between the fluid and the structure surface traction, respectively. The inverse $\tilde{P}_U^{-1}$ is given by

$$\tilde{P}_U^{-1} = \begin{bmatrix} \tilde{A}_m^{-1} & 0 & -\tilde{A}_m^{-1} A_{ms} \tilde{A}_s^{-1} \\ & \tilde{A}_f^{-1} & -\tilde{A}_f^{-1} A_{fs} \tilde{A}_s^{-1} \\ & & \tilde{A}_s^{-1} \end{bmatrix}, \tag{25}$$

that is nothing but a Gauss-Seidel iteration using a backward substitution. As we see the block A_{fm} of the derivative of the fluid sub-problem with respect to the fluid domain displacement is not take into account.

4.1.4. *The SSOR−preconditioner.* We consider a Symmetric Successive Over-Relaxation (SSOR) with a special choice of the relaxation parameter $\omega = 1$. The preconditioner is based on the following LU factorization of P_{SSOR} given by

$$\begin{aligned} P_{SSOR} &= \begin{bmatrix} A_m & & \\ A_{fm} & A_f & \\ 0 & A_{sf} & A_s \end{bmatrix} \times \begin{bmatrix} I & 0 & A_m^{-1} A_{ms} \\ & I & A_f^{-1} A_{fs} \\ & & I \end{bmatrix} \\ &= \begin{bmatrix} A_m & 0 & A_{ms} \\ A_{fm} & A_f & A_{fs} + A_{fm} A_m^{-1} A_{ms} \\ 0 & A_{sf} & A_s + A_{sf} A_f^{-1} A_{fs} \end{bmatrix}. \end{aligned} \tag{26}$$

that can be reformulated as $P_{SSOR} = K + R_{SSOR}$, where the remainder R_{SSOR} is given by

$$R_{SSOR} = \begin{bmatrix} 0 & 0 & 0 \\ 0 & 0 & A_{fm} A_m^{-1} A_{ms} \\ 0 & 0 & A_{sf} A_f^{-1} A_{fs} \end{bmatrix}.$$

The $SSOR$ preconditioner $\tilde{P}_{SSOR}$ is then given by

$$\tilde{P}_{SSOR} = \begin{bmatrix} \tilde{A}_m & & \\ A_{fm} & \tilde{A}_f & \\ 0 & A_{sf} & \tilde{A}_s \end{bmatrix} \times \begin{bmatrix} I & 0 & \tilde{A}_m^{-1} A_{ms} \\ & I & \tilde{A}_f^{-1} A_{fs} \\ & & I \end{bmatrix}. \tag{27}$$

The inverse of $\tilde{P}_{SSOR}$ is computed by two block Gauss-Seidel iterations using the backward and forward substitution consecutively:

$$\tilde{P}_{SSOR}^{-1} = \begin{bmatrix} I & 0 & -\tilde{A}_m^{-1}A_{ms} \\ & I & -\tilde{A}_f^{-1}A_{fs} \\ & & I \end{bmatrix} \times \begin{bmatrix} \tilde{A}_m^{-1} & & \\ -\tilde{A}_f^{-1}A_{fm}\tilde{A}_m^{-1} & \tilde{A}_f^{-1} & \\ -\tilde{A}_s^{-1}A_{sf}\tilde{A}_f^{-1}A_{fm}\tilde{A}_m^{-1} & -\tilde{A}_s^{-1}A_{sf}\tilde{A}_f^{-1} & \tilde{A}_s^{-1} \end{bmatrix}. \tag{28}$$

Compared to $\tilde{P}_L^{-1}$ and $\tilde{P}_U^{-1}$, two more inverse operations of $\tilde{A}_m^{-1}$ and $\tilde{A}_f^{-1}$ are required.

4.1.5. *The $ILU(0)-$preconditioner.* We finally consider the $ILU(0)-$preconditioner $\tilde{P}_{ILU}$. This incomplete factorization technique is described in, e.g., [63, 20, 6]. Here we apply a block $ILU(0)$ factorization for the coupled FSI system given by

$$\begin{aligned} P_{ILU} &= \begin{bmatrix} I & & \\ A_{fm}A_m^{-1} & I & \\ 0 & A_{sf}A_f^{-1} & I \end{bmatrix} \times \begin{bmatrix} A_m & 0 & A_{ms} \\ & A_f & A_{fs} - A_{fm}A_m^{-1}A_{ms} \\ & & A_s \end{bmatrix} \\ &= \begin{bmatrix} A_m & 0 & A_{ms} \\ A_{fm} & A_f & A_{fs} \\ 0 & A_{sf} & A_s + A_{sf}A_f^{-1}(A_{fs} - A_{fm}A_m^{-1}A_{ms}) \end{bmatrix}, \end{aligned} \tag{29}$$

that can be rewritten as $P_{ILU} = K + R_{ILU}$, where the remainder R_{ILU} is given by

$$R_{ILU} = \begin{bmatrix} 0 & 0 & 0 \\ 0 & 0 & 0 \\ 0 & 0 & A_{sf}A_f^{-1}(A_{fs} - A_{fm}A_m^{-1}A_{ms}) \end{bmatrix}.$$

The preconditioner $\tilde{P}_{ILU}$ is then given by

$$\begin{aligned} \tilde{P}_{ILU} &= \begin{bmatrix} I & & \\ A_{fm}\tilde{A}_m^{-1} & I & \\ 0 & A_{sf}\tilde{A}_f^{-1} & I \end{bmatrix} \times \begin{bmatrix} \tilde{A}_m & 0 & A_{ms} \\ & \tilde{A}_f & A_{fs} - A_{fm}\tilde{A}_m^{-1}A_{ms} \\ & & \tilde{A}_s \end{bmatrix} \\ &= \begin{bmatrix} \tilde{A}_m & 0 & A_{ms} \\ A_{fm} & \tilde{A}_f & A_{fs} \\ 0 & A_{sf} & \tilde{A}_s + A_{sf}\tilde{A}_f^{-1}(A_{fs} - A_{fm}\tilde{A}_m^{-1}A_{ms}) \end{bmatrix}. \end{aligned} \tag{30}$$

The inverse of $\tilde{P}_{ILU}$ is then computed by two block Gauss-Seidel iterations using the forward and backward substitution consecutively:

$$\tilde{P}_{ILU}^{-1} = \begin{bmatrix} I & & \\ -A_{fm}\tilde{A}_m^{-1} & I & \\ A_{sf}\tilde{A}_f^{-1}A_{fm}\tilde{A}_m^{-1} & -A_{sf}\tilde{A}_f^{-1} & I \end{bmatrix} \times \begin{bmatrix} \tilde{A}_m^{-1} & 0 & -\tilde{A}_m^{-1}\tilde{A}_s^{-1} \\ & \tilde{A}_f^{-1} & -\tilde{A}_f^{-1}(A_{fs} - A_{fm}\tilde{A}_m^{-1}A_{ms}) \\ & & \tilde{A}_s^{-1} \end{bmatrix}. \tag{31}$$

Compared to $\tilde{P}_L^{-1}$ and $\tilde{P}_U^{-1}$, two more inverse operations of $\tilde{A}_m^{-1}$ and one more inverse operation of $\tilde{A}_f^{-1}$ are required.

4.2. **Algebraic multigrid method for the coupled FSI system.** The *LU* factorization is probably the best well-known preconditioner for solving general systems. Unfortunately, those preconditioners discussed in Section 4.1 for the FSI coupled system are not robust with respect to, e.g., the mesh size. As we observe from numerical experiments, the iteration numbers increase when the mesh is refined. In order to eliminate the mesh dependence, we consider the AMG and AMLI method. These methods tackles the low and high frequency errors separately by using the smoothing and coarse grid correction step. We discuss two essential components, the coarsening strategy and smoother, that are used in both the AMG and AMLI method.

4.2.1. *The coarsening strategy.* First of all, we define a full rank prolongation matrix

$$P_{l+1}^l = \begin{bmatrix} P_m^l & & \\ & P_f^l & \\ & & P_s^l \end{bmatrix}, \tag{32}$$

where $l = 1, ..., L-1$, indicates the levels of a hierarchy, i.e., index 1 refers to the finest level and L the coarsest level. Here $P_m^l : \mathbb{R}^{n_m^{l+1}} \mapsto \mathbb{R}^{n_m^l}$ denotes the prolongation matrix constructured for the elliptic mesh movement sub-problem as in [47], n_m^l the number of DOF of the mesh movement sub-problem on level l and $n_m^{l+1} < n_m^l$. In a similar way, $P_f : \mathbb{R}^{n_m^{l+1}} \mapsto \mathbb{R}^{n_m^l}$ and $P_s : \mathbb{R}^{n_s^{l+1}} \mapsto \mathbb{R}^{n_s^l}$ represent the prolongation matrices constructured for the indefinite fluid and structure sub-problem as in [73, 52], that take the stability into account by proper scaling and avoid a mixture of velocity/displacement and pressure components on coarse levels, n_f^l and n_s^l the number of DOF of the fluid and structure sub-problem on level l and $n_f^{l+1} < n_f^l$, $n_s^{l+1} < n_s^l$.

Then it is easy to see $P_{l+1}^{l} : \mathbb{R}^{n_m^{l+1}+n_f^{l+1}+n_s^{l+1}} \mapsto \mathbb{R}^{n_m^{l}+n_f^{l}+n_s^{l}}$. More sophisticated and expensive coarsening strategies of the AMG method for saddle point systems arising from the fluid sub-problem can be found in [54]. In this work, we restrict ourselves to the strategy introduced in [73], where a simple scaling technique is applied. We then define a restriction matrix $R_l^{l+1} : \mathbb{R}^{n_m^{l}+n_f^{l}+n_s^{l}} \mapsto \mathbb{R}^{n_m^{l+1}+n_f^{l+1}+n_s^{l+1}}$ as

$$R_l^{l+1} = \begin{bmatrix} R_m^{l+1} & & \\ & R_f^{l+1} & \\ & & R_s^{l+1} \end{bmatrix}, \tag{33}$$

where $R_m^{l+1} = (P_m^l)^T$, $R_f^{l+1} = (P_f^l)^T$ and $R_s^{l+1} = (P_s^l)^T$. The system on the finest level L is given by (18) that is formulated as $K_1 x_1 = b_1$. Then the system matrix on the coarse level $l+1$ is formulated by the Galerkin projection that has considered the stability of indefinite sub-systems on coarse levels:

$$K_{l+1} = R_l^{l+1} K_l P_{l+1}^l = \begin{bmatrix} R_m^{l+1} A_m^l P_m^l & 0 & R_m^{l+1} A_{ms}^l P_s^l \\ R_f^{l+1} A_{fm}^l P_m^l & R_f^{l+1} A_f^l P_f^l & R_f^{l+1} A_{fs}^l P_s^l \\ 0 & R_s^{l+1} A_{sf}^l P_f^l & R_s^{l+1} A_s^l P_s^l \end{bmatrix}, \tag{34}$$

where A_i^l, $i \in \{m, ms, fm, f, fs, sf, s\}$ denote the matrices on the level l, $l = 1, ..., L-1$. On the coarsest level L, the coupled system is solved by a direct solver.

4.2.2. *The smoother.* To complete the AMG method we need an iterative method (the smoother) for the problem $K_l x_l = b_l$, $l = 1, ..., L-1$,

$$x_l^{k+1} = \mathcal{S}_l(x_l^k, b_l) \tag{35}$$

with

$$x_l^k = \begin{bmatrix} \Delta d_{m,l}^k \\ \Delta u_{f,l}^k \\ \Delta u_{s,l}^k \end{bmatrix}, b_l = \begin{bmatrix} r_{m,l} \\ r_{f,l} \\ r_{s,l} \end{bmatrix}, \tag{36}$$

where k is the iteration index.

For this coupled FSI system, we consider the following preconditioned Richardson method, that turns out to be an effective FSI smoother with sufficient large number of smoothing steps: For $k \geq 0$,

$$\begin{bmatrix} \Delta d_{m,l}^{k+1} \\ \Delta u_{f,l}^{k+1} \\ \Delta u_{s.l}^{k+1} \end{bmatrix} = \begin{bmatrix} \Delta d_{m,l}^{k} \\ \Delta u_{f,l}^{k} \\ \Delta u_{s.l}^{k} \end{bmatrix} + P_{Rich}^{-1} \left(\begin{bmatrix} r_{m,l} \\ r_{f,l} \\ r_{s.l} \end{bmatrix} - K_l \begin{bmatrix} \Delta d_{m,l}^{k} \\ \Delta u_{f,l}^{k} \\ \Delta u_{s.l}^{k} \end{bmatrix} \right), \tag{37}$$

where the preconditioner is given by

$$P_{Rich} = \begin{bmatrix} \frac{1}{\omega_m}\tilde{A}_m^l & & \\ A_{fm}^l & \frac{1}{\omega_f}\tilde{A}_f^l & \\ 0 & A_{sf}^l & \frac{1}{\omega_s}\tilde{A}_s^l \end{bmatrix} \tag{38}$$

with the scaled block diagonal matrices. The inverse of each of these matrices is realized by applying one AMG cycle to each sub-problem, that has been developed in our previous work [52]. In principle, these damping parameters ω_i, $i \in \{m, f, s\}$, may be chosen differently. For simplicity, we use $\omega_m = \omega_f = \omega_s = \omega$ in our numerical experiments. This FSI smoother shows numerical robustness with respect to different hyperelastic models considered in the coupled FSI system and the AMG levels, i.e., the same damping parameter ω has been used in our numerical experiments. It is easy to see, one iteration of the preconditiond Richardson method consists of three steps of the following damped block Gauss-Seidel like iteration, that is demonstrated in Algorithm 2.

Algorithm 2 Block Gauss-Seidel iteration: $x_l^{k+1} = \mathcal{S}_l(x_l^k, b_l)$

Given initial x_l^k,

1: $\Delta d_{m,l}^{k+1} = \Delta d_{m,l}^k + \omega_m(\tilde{A}_m^l)^{-1}(r_{m,l} - A_m^l \Delta d_{m,l}^k - A_{ms}^l \Delta u_{s,l}^k)$,

2: $\Delta u_{f,l}^{k+1} = \Delta u_{f,l}^k + \omega_f(\tilde{A}_f^l)^{-1}(r_{f,l} - A_{fm}^l \Delta d_{m,l}^{k+1} - A_f^l \Delta u_{f,l}^k - A_{f,s}^l \Delta u_{s,l}^k)$,

3: $\Delta u_{s.l}^{k+1} = \Delta u_{s,l}^k + \omega_s(\tilde{A}_s^l)^{-1}(r_{s,l} - A_{sf}^l \Delta u_{f,l}^{k+1} - A_s^l \Delta u_{s,l}^k)$.

4.2.3. *The algebraic multigrid iteration.* The basic AMG iteration is given in Algorithm 3, where m_{pre} and m_{post} refer to the number of pre- and post-smoothing steps. For $\nu = 1$ and $\nu = 2$, the iterations in Algorithm 3 are called V- and W-cycle, respectively. In our numerical experiments, we choose the W-cycle. On the coarsest level L, we use direct solver to handle the coupled system.

As seen from Algorithm 3, steps 1-3 and steps 14-16 correspond to the presmoothing and postsmoothing, respectively, steps 4-13 are referred to as "coarse grid correction". The full AMG iterations are realized by repeated application of this algorithm until it satisfies certain stopping criteria. The iteration in this algorithm is also combined with GMRES [64] and FGMRES [62] methods, that leads to fast convergence of the preconditioned Krylov subspace methods for the coupled FSI system.

Algorithm 3 Basic AMG iteration: AMG(K_l, x_l, b_l)

1: **for** $k = 1$ to m_{pre} **do**
2: $x_l^{k+1} = \mathcal{S}_l(x_l^k, b_l)$
3: **end for**
4: $b_{l+1} = R_l^{l+1}(b_l - K_l x_l)$,
5: **if** l+1=L **then**
6: Solve $K_L x_L = b_L$
7: **else**
8: $x_{l+1} = 0$,
9: **for** $k = 1, ..., \nu$ **do**
10: x_{l+1} =AMG($K_{l+1}, x_{l+1}, b_{l+1}$),
11: **end for**
12: **end if**
13: $x_l = x_l + P_{l+1}^l x_{l+1}$,
14: **for** $k = 1$ to m_{post} **do**
15: $x_l^{k+1} = \mathcal{S}_l(x_l^k, b_l)$,
16: **end for**
17: return x_l.

4.3. **Algebraic multilevel method for the coupled FSI system.** The AMLI method [5, 7, 72, 50], sometimes referred to as "K-cycle", is viewed as a W-cycle with the Krylov acceleration at the intermediate levels; see, e.g. [57, 59, 3, 72]. Here we combine our monolithic AMG method with the FGMRES Krylov subspace method at the intermediate levels, i.e., we reuse the coarsening strategy and smoothers constructed for the FSI AMG method. Instead of calling the AMG cycle (steps 9-10 in Algorithm 3), the AMLI algorithm calls the AMLI cycle recursively ν times as a preconditioner inside the FGMRES method for the coarse grid correction equations; see step 9 in Algorithm 4.

It is easy to see, this method represents a variant of the W-cycle AMG method in the case of $\nu = 2$; see an illustration for such W-cyles with 3 levels ($L = 3$) in Fig. 2. Compared to the AMG W-cycle, the two preconditioned FGMRES iterations are called consecutively on the second level of the AMLI W-cycle, that are used to accelerate the convergence rate.

5. Numerical experiments

5.1. **Material and geometrical data, meshes and boundary conditions.** We use the geometrical data from [21, 42]; see an illustration in Fig.3. In order to compare FSI simulation using different hyperelastic models (see Section 2.3), we adopt the same geometrical data

Algorithm 4 Basic AMLI iteration: AMLI(K_l, x_l, b_l)

for $k = 1$ to m_{pre} **do**
  $x_l^{k+1} = \mathcal{S}_l(x_l^k, b_l)$
end for
$b_{l+1} = R_l^{l+1}(b_l - K_l x_l)$,
if l+1=L **then**
  Solve $K_L x_L = b_L$
else
  $x_{l+1} = 0$,
  FGMRES(K_{l+1}, x_{l+1}, b_{l+1}, ν, AMLI),
end if
$x_l = x_l + P_{l+1}^l x_{l+1}$,
for $k = 1$ to m_{post} **do**
  $x_l^{k+1} = \mathcal{S}_l(x_l^k, b_l)$,
end for
return x_l.

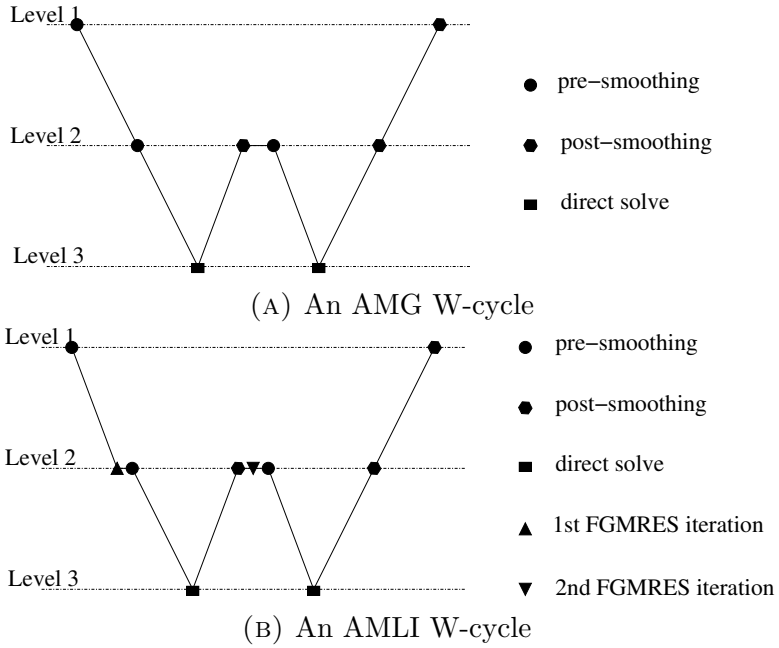

(A) An AMG W-cycle

(B) An AMLI W-cycle

FIGURE 2. An illustration of W-cycles for the AMG and AMLI methods with 3 levels.

(except the angles α_M and α_A) for the models of Neo-Hookean and Mooney-Rivlin materials. Furthermore, we set the value of the material parameters for three hyperelastic models as indicated in Tab. 1,

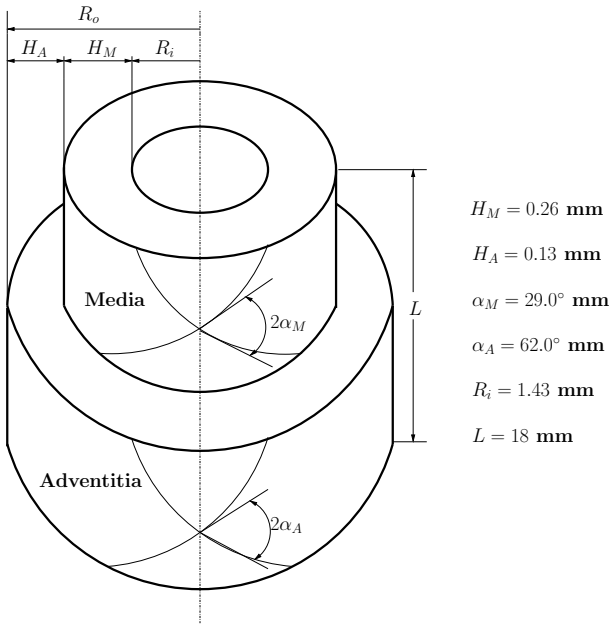

FIGURE 3. Geometrical data for a carotid artery from a rabbit (see [42, 21])

where M denotes the media and A the adventitia. We use Netgen

	c_{10}		c_{01}		ρ_s
	M	A	M	A	
Neo-Hookean	3 kPa	0.3 kPa	–	–	1.2 kg/m^3
Mooney-Rivlin	3 kPa	0.3 kPa	0.3 kPa	0.2 kPa	1.2 kg/m^3
Artery	3 kPa	0.3 kPa	–	–	1.2 kg/m^3
	k_1		k_2		κ
	M	A	M	A	
Neo-Hookean	–	–	–	–	10^5 kPa
Mooney-Rivlin	–	–	–	–	10^5 kPa
Artery	2.3632 kPa	0.5620 kPa	0.8393	0.7112	10^5 kPa

TABLE 1. The value of material parameters for three hyperelastic models.

[66] to generate finite element mesh for the computational FSI domain, that provides conforming grids on the FSI interface and two-layered structure interface. In order to study the robustness of the solvers (see

Section 4) for the linearized coupled FSI system with respect to the discretization mesh parameter, three finite element meshes are generated using Netgen. In Tab. 2, we summarize the total number of grid nodes (#Nod), tetrahedra (#Tet) and degrees of freedom (#Dof) in the finite element simulation, that includes the mesh movement, fluid and structure sub-problems. For the fluid, we set the density $\rho_f = 1$

	#Nod	#Tet	#Dof
Coarse mesh	1034	4824	6959
Intermediate mesh	7249	38592	37909
Fine mesh	54521	308736	285167

TABLE 2. Three finite element meshes.

mg/mm^3, the dynamic viscosity $\mu = 0.035$ Poise. The fluid Neumann boundary condition on Γ_{in}^t is given by $g_{in} = 1.332 n_f$ kPa for $t \leq 0.125$ ms and $g_{in} = 0$ kPa for $t > 0.125$ ms. The remaining boundary conditions are specified in Section 2. The fluid and structure are at the rest in the initial time. The time step size Δt is set to 0.125 ms. We run the simulation until 12 ms.

5.2. **Convergence of Newton's method.** To verify the linearization for the coupled nonlinear FSI system (see Section 3.4), we show the relative error (err) and iteration number (#it) of Newton's method for the FSI simulation using three different hyperelastic models: Neo-Hookean (FSI_NH), Mooney-Rivlin (FSI_MR) and artery (FSI_AR), and three different meshes: Coarse mesh (C), intermediate mesh (I) and fine mesh (F); see Tab. 3 for details. Note that since we observe the same performance of Newton's method for solving the nonlinear system at all time steps, only the performance at the first time step is recorded in Tab. 3 for simplicity of presentation. From the convergence history displayed in Tab. 3, we observe (near)quadratic convergence rate of Newton's method, that conforms the derivation for the linearization of the coupled nonlinear FSI system, stemming from the domain movements, convection terms, material laws, transmission conditions and stabilization parameters. We observe nearly the same convergence rate for the nonlinear FSI system using three different hyperelastic models on the coarse, intermediate and fine mesh. At each iteration of Newton's method, we use the preconditioned Krylov subspace, algebraic multigrid and multilevel methods to solve the linearized FSI system; see numerical results in Section 5.3 and 5.4.

FSI_NH:			
#it	err		
	C	I	F
1	$6.2e+01$	$6.8e+01$	$6.9e+01$
2	$3.8e-02$	$5.7e-02$	$6.6e-02$
3	$7.4e-06$	$7.7e-06$	$4.0e-06$
4	$4.3e-09$	$1.1e-09$	$1.3e-08$
FSI_MR:			
#it	err		
	C	I	F
1	$6.2e+01$	$6.8e+01$	$6.9e+01$
2	$3.8e-02$	$5.7e-02$	$6.4e-02$
3	$7.3e-06$	$7.3e-06$	$3.0e-06$
4	$4.3e-09$	$9.7e-10$	$2.5e-09$
FSI_AR:			
#it	err		
	C	I	F
1	$6.2e+01$	$6.8e+01$	$6.9e+01$
2	$4.0e-02$	$6.0e-02$	$7.0e-02$
3	$7.5e-06$	$8.4e-06$	$1.2e-05$
4	$4.3e-09$	$1.2e-09$	$4.0e-09$

TABLE 3. The convergence history of Newton's method for the FSI nonlinear system using three hyperelastic models and meshes.

5.3. **Iteration numbers of preconditioned Krylov subspace methods.** To compare performance of preconditioned Krylov subspace methods for the linearized coupled FSI system, we use the GMRES method combined with the preconditioners from Section 4.1. The stopping criterion for the GMRES method is set by the relative error 10^{-9}. We compare the total number of GMRES iterations (#it) to reach this criterion for the FSI simulation using the Neo-Hookean (FSI_NH), Mooney-Rivlin (FSI_MR) and artery (FSI_AR) model on coarse mesh (C), intermediate mesh (I) and fine mesh (F). The detailed numerical results are shown in Tab. 4. Note that since the performance is similar

for all Newton iterations, we demonstrate the iteration numbers at the first Newton iteration. The inverse of each sub-problem in the preconditioners is realized by calling the corresponding AMG cycle, that has been developed in [52]. As we observe from the iteration numbers of

Precontitioner	#it								
	FSI_NH			FSI_MR			FSI_AR		
	C	I	F	C	I	F	C	I	F
$\tilde{P}_D$	51	111	217	53	111	227	46	98	189
$\tilde{P}_L$	28	58	109	29	60	114	25	50	95
$\tilde{P}_U$	28	59	114	28	61	119	25	51	98
$\tilde{P}_{SSOR}$	27	54	104	28	57	108	24	48	91
$\tilde{P}_{ILU}$	27	54	104	28	57	108	24	48	91

TABLE 4. The performance of preconditioned GMRES method for the linearized FSI system using three hyperelastic models and meshes.

the linear solvers using different preconditioners in Tab. 4, the solver with the preconditioner $\tilde{P}_D$ requires more iteration numbers than the other four preconditioners. The solvers with the preconditioners $\tilde{P}_L$, $\tilde{P}_U$, $\tilde{P}_{SSOR}$ and $\tilde{P}_{ILU}$ require almost the same number of iteration numbers. As expected, when the mesh is refined, the iteration number of the preconditioned GMRES method increases. We will see in Section 5.4 that, the mesh dependence is eliminated by using the multigrid and multilevel method.

5.4. **Iteration numbers of algebraic multigrid and multilevel methods.** In this section, we compare the performance of the AMG and AMLI method for the linearized coupled FSI system. More precisely, we show the number of iteration numbers (#it) of the AMG, AMLI, AMG preconditioned GMRES (AMG_GMRES), AMG preconditioned FGMRES (AMG_FGMRES), AMLI preconditioned GMRES (AMLI_GMRES) and AMLI preconditioned FGMRES (AMLI_FGMRES) method, respectively, up to the relative error 10^{-9}. We run the FSI simulation using the Neo-Hookean (FSI_NH), Mooney-Rivlin (FSI_MR), artery (FSI_AR) model, on the coarse (C), intermediate (I) and fine (F) mesh, respectively. See Tab. 5 for details. We use $8-10$ smoothing steps in the AMG and AMLI cycle, each of which only requires 1 AMG cycle for the corresponding mesh movement, fluid and structure

sub-problem (see Section 4.2.2). As preconditioners, we only apply 1 AMG or AMLI cycle in the preconditioned GMRES or FGMRES iteration. As we observe from Tab. 5, the AMG and AMLI method

Method	#it								
	FSI_NH			FSI_MR			FSI_AR		
	C	I	F	C	I	F	C	I	F
AMG	7	8	12	8	8	11	7	8	10
AMG_GMRES	7	7	8	7	7	8	7	7	8
AMG_FGMRES	6	7	8	6	7	9	6	7	8
AMLI	7	8	12	8	8	11	7	8	10
AMLI_GMRES	7	7	8	7	7	8	7	7	8
AMLI_FGMRES	6	7	8	6	7	9	6	7	8

TABLE 5. The performance of the AMG, AMLI, and AMG and AMLI preconditioned Krylov subspace method for the linearized FSI system using three hyperelastic models and meshes.

requires the same iteration numbers for each case. The AMG and AMLI preconditioned GMRES and FGMRES methods show improved performance with fewer iteration numbers than the AMG and AMLI methods. When the mesh is refined, we observe the iteration numbers using these methods stay in a very similar range. This demonstrates the robustness of the multigrid and multilevel method for the coupled FSI system with respect to the mesh refinement.

5.5. **Visualization of the numerical solutions.** In order to demonstrate the numerical simulation results, we visualize the structure deformations and fluid velocity fields in Fig. 4, where the FSI solutions at time level $t = 8$ ms using the structure models of the Neo-Hookean material, the Mooney-Rivlin material and the anisotropic two-layer thick walled artery, are respectively shown.

5.6. **Comparison with the partitioned approach.** In this section, we compare the numerical simulation results obtained by the monolithic approach with the results by the partitioned approach as in [52].

We first compare the fluid pressure waves obtained from the FSI simulation using different structure models. In Fig. 5, Fig. 6 and Fig. 7, we plot fluid pressure waves along the center line with the starting

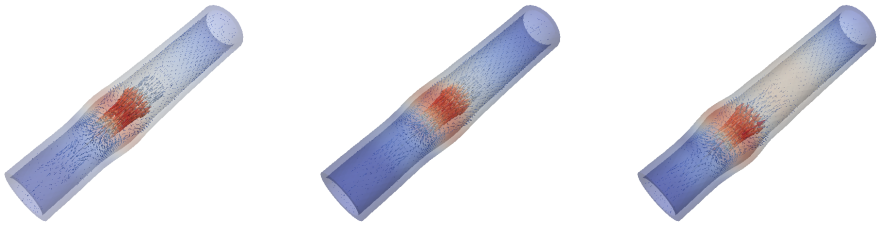

(A) Neo-Hookean (B) Mooney-Rivlin (C) Artery

FIGURE 4. Visualization of structure deformation and fluid velocity fields at time $t = 8$ ms using three different structure models of Neo-Hookean material (left), Mooney-Rivlin material (middle) and anisotropic two-layer thick walled artery.

point $(0, 0, 0)$ cm and ending point $(0, 0, 1.8)$ cm, for the model of Neo-Hookean material, Mooney-Rivlin material and anisotropic two-layer thick walled artery, respectively. In each subplot of these three figures, the horizontal line represents the center line (in cm), and the vertical line represents the pressure (in Pa).

We compare the pressure waves at different time levels using the monolithic and partitioned approach. According to our experiments, we observe at the first time steps, the solution obtained by using the monolithic and partitioned approach conforms to each other very well. With time stepping, the solution obtained by the partitioned approach has smaller magnitude than the solution by the monolithic approach. This is due to the fact that, at each time level of the partitioned approach, we apply the fixed-point method to the reduced interface equation in an iterative manner, which introduce some additional errors in the solution procedure. These additional errors are accumulated with time stepping. However, for the monolithic approach, we solve the coupled system in an all-at-once manner, such additional errors are eliminated.

Secondly, in order to see the effects of different structure models applied in the FSI simulation, we also compare the fluid pressure waves extracted from the FSI simulation using the model of Neo-Hookean material (solid lines), Mooney-Rivlin material (dashed lines) and anisotropic two-layer thick walled artery (dash dotted lines) in Fig. 8, where the horizontal line represents the center line (in cm), and the vertical line represents the pressure (in Pa). As we observe, the simulation results obtained from the model of Neo-Hookean and Mooney-Rivlin material are quite similar to each other (the speed and magnitude of the

pressure waves). This is due to the fact that these two models have only one term difference in the energy functional; see (2) and (4). The pressure waves obtained from the model of the anisotropic two-layer thick walled artery travels with slower speed and smaller magnitude than the other two models.

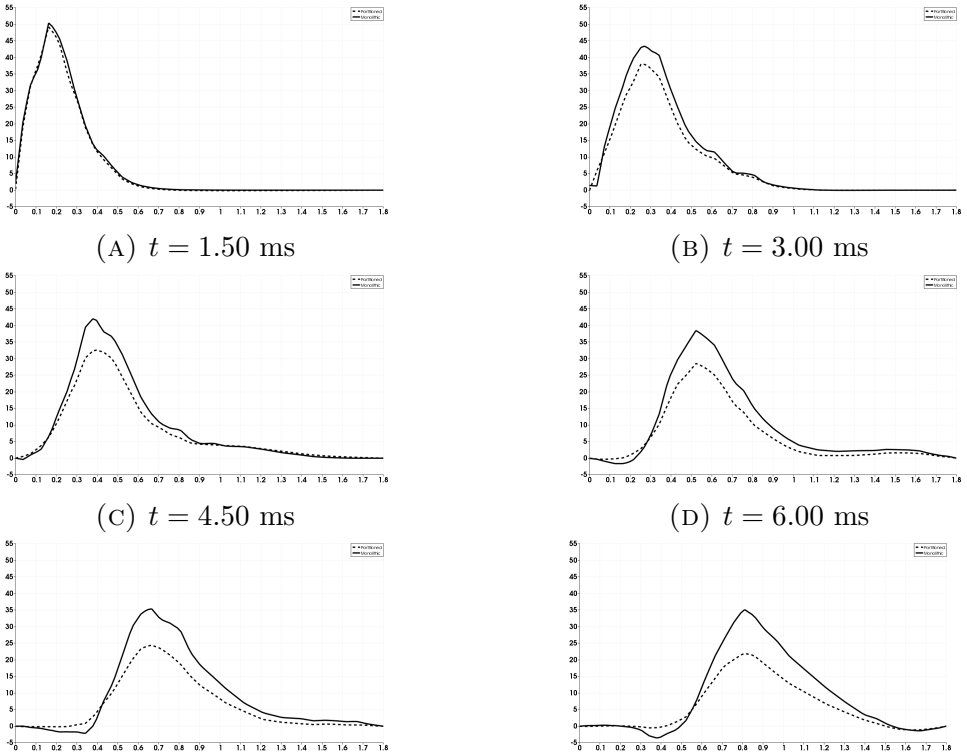

(A) $t = 1.50$ ms (B) $t = 3.00$ ms

(C) $t = 4.50$ ms (D) $t = 6.00$ ms

(E) $t = 7.50$ ms (F) $t = 9.00$ ms

FIGURE 5. Comparison of fluid pressure waves along the center line with the starting point $(0, 0, 0)$ cm and ending point $(0, 0, 1.8)$ cm from the FSI simulation using the model of Neo-Hookean material: Monolithic solution (in solid lines) and partitioned solution (in dashed lines).

As we discussed in [52], for the partitioned approach, we need around $50 \sim 55$ fixed-point iterations at each time step; for the monolithic approach we need about 4 Newton iterations. In each fixed-point iteration, we need about $4 - 5$ Newton iterations for solving the fluid and structure sub-problems; and in each Newton iteration, we apply the AMG sub-problem solvers for the linearized systems. For each Newton iteration in the monolithic approach, we need about 10 coupled AMG or AMLI iterations; and each coupled AMG or AMLI iteration requires

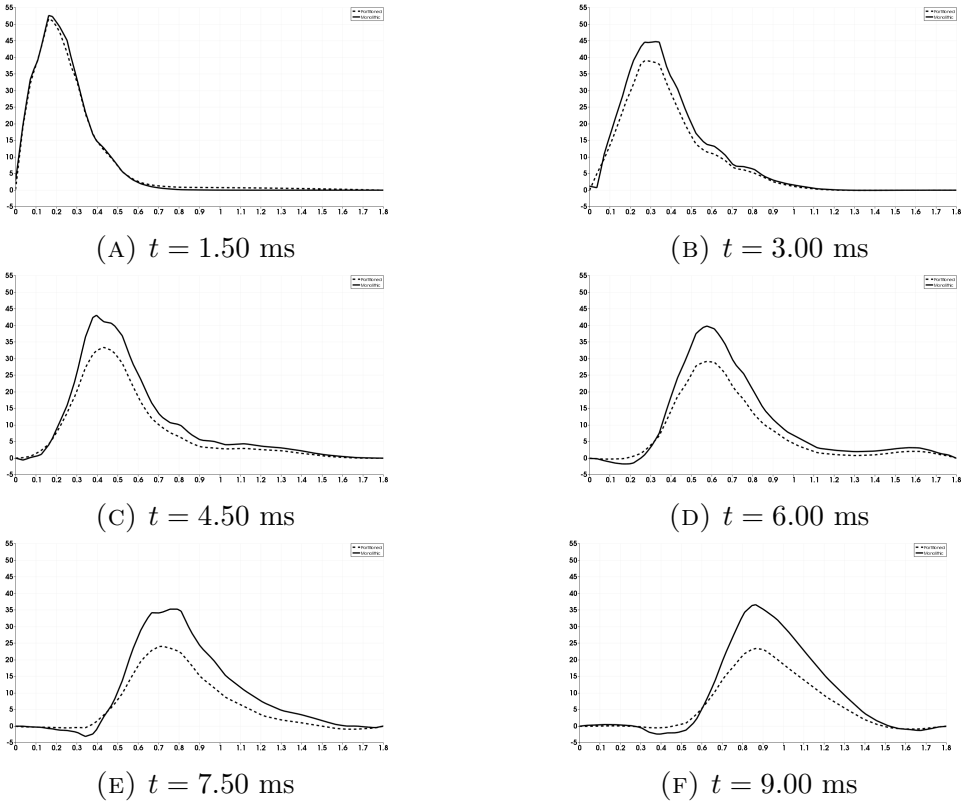

(A) $t = 1.50$ ms (B) $t = 3.00$ ms

(C) $t = 4.50$ ms (D) $t = 6.00$ ms

(E) $t = 7.50$ ms (F) $t = 9.00$ ms

FIGURE 6. Comparison of fluid pressure waves along the center line with the starting point $(0, 0, 0)$ cm and ending point $(0, 0, 1.8)$ cm from the FSI simulation using the modified model of Mooney-Rivlin material: Monolithic solution (in solid lines) and partitioned solution (in dashed lines).

apply one iteration of AMG sub-problem solvers. Altogether we observe almost 50% saving of the computational cost in the monolithic approach in comparison with the partitioned approach. Further reduction in computational cost will be realized by using parallel computing, see, e.g, [28], that is considered as a forthcoming work.

6. Conclusions

In this work, we have developed the monolithic approach for solving the coupled FSI problem in an all-at-once manner. The Newton method for the nonlinear coupled system demonstrates its robustness and efficiency. For solving the linearized FSI system, the preconditioned Krylov sub-space, algebraic multigrid and algebraic multilevel

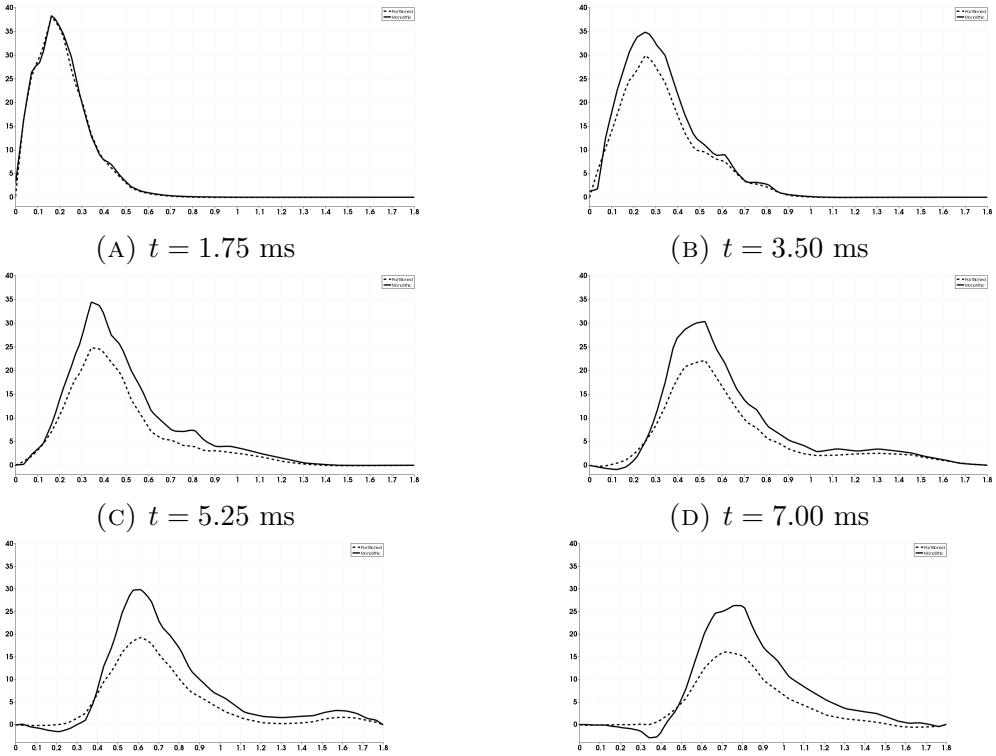

(A) $t = 1.75$ ms (B) $t = 3.50$ ms

(C) $t = 5.25$ ms (D) $t = 7.00$ ms

(E) $t = 8.75$ ms (F) $t = 10.50$ ms

FIGURE 7. Comparison of fluid pressure waves along the center line with the starting point $(0, 0, 0)$ cm and ending point $(0, 0, 1.8)$ cm from the FSI simulation using the anisotropic two-layer thick walled artery: Monolithic solution (in solid lines) and partitioned solution (in dashed lines).

methods have shown their good performance and robustness. In particular, the monolithic AMG and AMLI methods show more robustness than the preconditioned Krylov sub-space methods utilizing block factorization of the coupled system, i.e., the iteration numbers stay in a same range with the mesh refinement. Compare to the partitioned approach, the monolithic approach developed in the work shows its more robustness and efficiency with respect to the numerical results and solution methods.

REFERENCES

[1] R. ADAMS AND J. FOURNIER, *Sobolev Spaces*, Academic Press, Amsterdam, Boston, 2003.

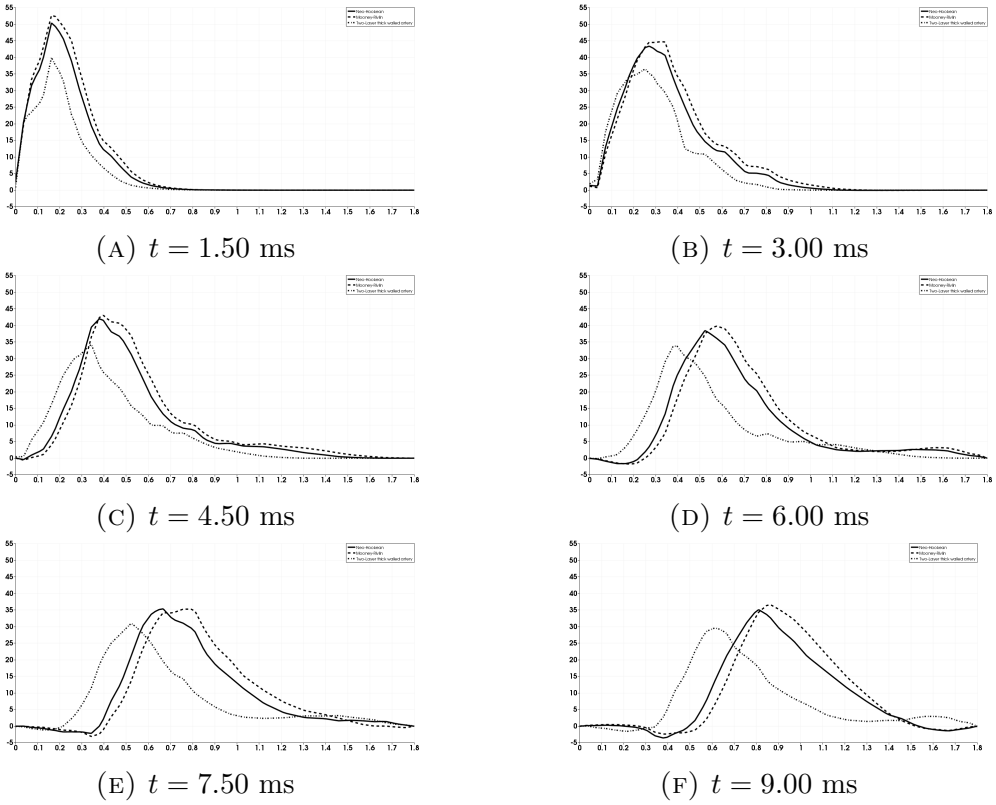

(A) $t = 1.50$ ms (B) $t = 3.00$ ms

(C) $t = 4.50$ ms (D) $t = 6.00$ ms

(E) $t = 7.50$ ms (F) $t = 9.00$ ms

FIGURE 8. Comparison of fluid pressure waves along the center line with the starting point $(0, 0, 0)$ cm and ending point $(0, 0, 1.8)$ cm from the FSI simulation using the model of Neo-Hookean material (in solid lines), the Mooney-Rivlin material (in dashed lines) and two-layer thick walled artery (in dash dotted lines).

[2] M. ÁNGEL FERNÁNDEZ AND M. MOUBACHIR, *A newton method using exact jacobians for solving fluidstructure coupling*, Comput. Structures, 83 (2005), pp. 127–142.

[3] A. APOSPORIDIS, P. S. VASSILEVSKI, AND A. VENEZIANI, *Multigrid preconditioning of the non-regularized augmented Bingham fluid problem*, Electron. Trans. Numer. Anal., 41 (2014), pp. 42–61.

[4] C. M. AUGUSTIN, G. A. HOLZAPFEL, AND O. STEINBACH, *Classical and all-floating FETI methods for the simulation of arterial tissues*, Int. J. Numer. Meth. Engng., 99 (2014), pp. 290–312.

[5] O. AXCLSSON AND P. VASSILEVSKI, *Algebraic multilevel preconditioning methods. I*, Numer. Math., 56 (1989), pp. 157–177.

[6] O. AXELSSON, *Iterative Solution Methods*, Cambridge Unveirstiy Press, New York, 1996.

[7] O. Axelsson and P. S. Vassilevski, *Algebraic multilevel preconditioning methods, II*, SIAM J. Numer. Anal., 27 (1990), pp. 1569–1590.
[8] S. Badia, F. Nobile, and C. Vergara, *Robin-Robin preconditioned Krylov methods for fluid-structure interaction problems*, Comput. Methods Appl. Mech. Engrg., 198 (2009), pp. 1768–2784.
[9] S. Badia, A. Quaini, and A. Quarteroni, *Modular vs. non-modular preconditioners for fluid-structure systems with large added-mass effect*, Comput. Methods Appl. Mech. Engrg., 197 (2008), pp. 4216–4232.
[10] J. Ball, *Convexity conditions and existence theorems in nonlinear elasticity*, Arch. Rational Mech. Anal., 63 (1976), pp. 337–403.
[11] A. Barker and X. Cai, *Scalable parallel methods for monolithic coupling in fluid-structure interaction with application to blood flow modeling*, J. Comput. Phys., (2010), pp. 642–659.
[12] A. Barker and X. Cai, *Two-level newton and hybrid schwarz preconditioners for fluid-structure interaction*, SIAM J. Sci. Comput., 32 (2010), pp. 2395–2417.
[13] J. Bayer, R. Blake, G. Plank, and N. Trayanova, *A novel rule-based algorithm for assigning myocardial fiber orientation to computational heart models*, Ann. Biomed. Eng., 40 (2012), pp. 2243–2254.
[14] Y. Bazilevs, V. Calo, T. Hughes, and Y. Zhang, *Isogeometric fluid-structure interaction: theory, algorithms, and computations*, Comput. Mech., 43 (2008), pp. 3–37.
[15] C. Bertoglio, P. Moireau, and J. Gerbeau, *Sequential parameter estimation for fluid-structure problems: Application to hemodynamics*, Int. J. Numer. Meth. Biomed. Engng., 28 (2012), pp. 434–455.
[16] J. Bonet and R. Wood, *Nonlinear Continuum Mechanics for Finite Element Analysis*, Cambridge University Press, New York, 2008.
[17] D. Braess and R. Sarazin, *An efficient smoother for the stokes problem*, Appl. Numer. Math., 23 (1997), pp. 3–19.
[18] F. Brezzi and M. Fortin, *Mixed and Hybrid Finite Element Methods*, Springer, New York, 1991.
[19] A. Brooks and T. Hughes, *Streamline upwind/Petrov-Galerkin formulations for convection dominated flows with particular emphasis on the incompressible Navier-Stokes equations*, Comput. Methods Appl. Mech. Engrg., 32 (1982), pp. 199–259.
[20] T. Chan and H. Vorst, *Approximate and incomplete factorizations*, in Parallel Numerical Algorithms, D. Keyes, A. Sameh, and V. Venkatakrishnan, eds., vol. 4 of ICASE/LaRC Interdisciplinary Series in Science and Engineering, 1997, pp. 167–202.
[21] C. Chuong and Y. Fung, *Three-dimensional stress distribution in arteries*, J. Biomech. Engr., 105 (1993), pp. 268–274.
[22] P. Ciarlet, *Mathematical Elasticity Volume I: Three-Dimensional Elasticity*, North-Holland, New York, 1988.
[23] P. Crosetto, S. Deparis, G. Fourestey, and A. Quarteroni, *Parallel algorithms for fluid-structure interaction problems in haemodynamics*, SIAM J. Sci. Comput., 33 (2011), pp. 1598–1622.

[24] S. Deparis, M. Discacciati, G. Fourestey, and A. Quarteroni, *Fluid-structure algorithms based on Steklov-Poincaré operators*, Comput. Methods Appl. Mech. Engrg., 195 (2006), pp. 5797–5812.

[25] W. Dettmer and D. Perić, *A computational framework for fluid-structure interaction: Finite element formulation and applications*, Comput. Methods. Appl. Mech. Engrg., 195 (2006), pp. 5754–5779.

[26] P. Deuflhard, *Newton Methods for Nonlinear Problems*, Springer, Heidelberg, 2005.

[27] J. Donea, A. Huerta, J. Ponthot, and A. Ferran, *Arbitrary Lagrangian-Eulerian methods*, in The Encyclopedia of Computational Mechanics, E. Stein, R. Borst, and T. Hughes, eds., vol. 1, Wiley& Sons, Ltd, 2004, pp. 413–437.

[28] C. C. Douglas, G. Haase, and U. Langer, *A Tutorial on Elliptic PDE Solvers and Their Parallelization*, SIAM, Philadelphia, 2003.

[29] M. A. Fernández, J. F. Gerbeau, and C. Grandmont, *A projection semi-implicit scheme for the coupling of an elastic structure with an incompressible fluid*, Int. J. Numer. Meth. Engng., 69 (2007), pp. 794–821.

[30] L. Formaggia and F. Nobile, *A stability analysis for the arbitrary Lagrangian Eulerian formulation with finite elements*, East-West J. Numer. Math., 7 (1999), pp. 105–132.

[31] C. Förster, *Robust methods for fluid-structure interaction with stabilised finite elements*, PhD thesis, University Stuttgart, 2007.

[32] C. Förster, W. Wall, and E. Ramm, *Stabilized finite element formulation for incompressible flow on distorted meshes*, Int. J. Numer. Meth. Fluids, 60 (2009), pp. 1103–1126.

[33] T. Gasser, R. Ogden, and G. Holzapfel, *Hyperelastic modelling of arterial layers with distributed collagen fibre orientations*, J. R. Soc. Interface, 3 (2006), pp. 15–35.

[34] M. W. Gee, U. Küttler, and W. A. Wall, *Truly monolithic algebraic multigrid for fluid-structure interaction*, Int. J. Numer. Meth. Engng., 85 (2011), pp. 987–1016.

[35] V. Girault and P. A. . Raviart, *Finite Element Methods for Navier-Stokes Equations*, Springer, Heidelberg, 1986.

[36] S. Goenezen, P. Barbone, and A. A. Oberai, *Solution of the nonlinear elasticity imaging inverse problem: The incompressible case*, Comput. Methods Appl. Mech. Engrg., 200 (2011), pp. 1406–1420.

[37] G. Haase and U. Langer, *Modern Methods in Scientific Computing and Applications*, vol. 75 of NATO Science Series II. Mathematics, Physics and Chemistry, Kluwer Academic Press, Dordrecht, 2002, ch. Multigrid Methods: From Geometrical to Algebraic Versions, pp. 103–154.

[38] C. Habchi, S. Russeil, D. Bougeard, J. L. Harion, T. Lemenand, A. Ghanem, D. D. Valle, and H. Peerhossaini, *Partitioned solver for strongly coupled fluid-structure interaction*, Comput. Fluids, 71 (2013), pp. 306–319.

[39] W. Hackbusch, *Multi-Grid Methods and Applications*, Springer, Heidelberg, 2003.

[40] M. Heil, *An efficient solver for the fully coupled solution of large-displacement fluid-structure interaction problems*, Comput. Methods Appl. Mech. Engrg., 193 (2004), pp. 1–23.

[41] G. Holzapfel, *Nonlinear Solid Mechanics: A Continuum Approach for Engineering*, John Wiley & Sons, Chichester, 2000.

[42] G. Holzapfel, T. Gasser, and R. Ogden, *A new constitutive framework for arterial wall mechanics and a comparative study of material models*, J. Elasticity, 61 (2000), pp. 1–48.

[43] M. Hsu and Y. Bazilevs, *Blood vessel tissue prestress modeling for vascular fluid-structure interaction simulation*, Finite Elem. Anal. Des., 47 (2011), pp. 593–599.

[44] T. Hughes, L. Franca, and G. Hulbert, *A new finite element formulation for computational fluid dynamics: VIII. The galerkin/least-squares method for advective-diffusive equations*, Comput. Methods Appl. Mech. Engrg., 73 (1989), pp. 173–189.

[45] T. Hughes, W. Liu, and T. Zimmermann, *Lagrangian-eulerian finite element formulation for incompressible viscous flows*, Comput. Methods Appl. Mech. Engrg., 29 (1981), pp. 329–349.

[46] M. Jung, U. Langer, A. Meyer, W. Queck, and M. Schneider, *Multigrid preconditioners and their applications*, in Third Multigrid Seminar, Biesenthal 1988, G. Telschow, ed., no. Report R–MATH–03/89, Berlin, 1989, Karl–Weierstrass–Institut, pp. 11–52.

[47] F. Kickinger, *Algebraic multigrid for discrete elliptic second-order problems*, in Multigrid Methods V. Proceedings of the 5th European Multigrid conference (ed. by W. Hackbush), Lecture Notes in Computational Sciences and Engineering, vol. 3, Springer, 1998, pp. 157–172.

[48] O. Klaas, A. Maniatty, and M. Shephard, *A stabilized mixed finite element method for finite elasticity.: Formulation for linear displacement and pressure interpolation*, Comput. Methods Appl. Mech. Engrg., 180 (1999), pp. 65–79.

[49] J. Kraus, *Additive Schur complement approximation and application to multilevel preconditioning*, SIAM J. Sci. Comput., 34 (2012), pp. A2872–A2895.

[50] J. Kraus and S. Margenov, *Robust Algebraic Multilevel Methods and Algorithms*, vol. 5 of Radon Series on Computational and Applied Mathematics, Walter de Gruyter, Berlin, New York, 2009.

[51] U. Küttler and W. Wall, *Fixed-point fluid-structure interaction solvers with dynamic relaxation*, Comput. Mech., 43 (2008), pp. 61–72.

[52] U. Langer and H. Yang, *Partitioned solution algorithms for fluid-structure interaction problems with hyperelastic models*, J. Comput. Appl. Math., (2014). accepted for publication, see also http://arxiv.org/abs/1312.5561.

[53] A. Maniatty, Y. Liu, O. Klaas, and M. Shephard, *Higher order stabilized finite element method for hyperelastic finite deformation*, Comput. Methods Appl. Mech. Engrg., 191 (2002), pp. 1491–1503.

[54] B. Metsch, *Algebraic Multigrid (AMG) for Saddle Point Systems*, PhD thesis, Rheinischen Friedrich-Wihelms-Universität Bonn, 2013.

[55] P. Moireau, C. Bertoglio, N. Xiao, C. Figueroa, C. Taylor, D. Chapelle, and J. Gerbeau, *Sequential identification of boundary support parameters in a fluid-structure vascular model using patient image data*, Biomech. Model Mechanobiol., 12 (2013), pp. 475–496.

[56] P. Moireau, N. Xiao, A. Astorino, C. Figueroa, D. Chapelle, C. Taylor, and J. Gerbeau, *External tissue support and fluid-structure simulation in blood flows*, Biomech. Model Mechanobiol., 11 (2012), pp. 1–18.

[57] A. C. Muresan and Y. Notay, *Analysis of aggregation-based multigrid*, SIAM J. Sci. Comput., 30 (2008), pp. 1082–1103.

[58] N. Newmark, *A method of computation for structural dynamics*, J. Eng. Mech., 85 (EM3) (1959), pp. 67–94.

[59] Y. Notay and P. S. Vassilevski, *Recursive Krylov-based multigrid cycles*, Numer. Lin. Alg. Appl., 15 (2008), pp. 473–487.

[60] W. Peter, *Nonlinear Finite Element Methods*, Springer, Heidelberg, 2008.

[61] M. Razzaq, H. Damanik, J. Hron, A. Ouazzi, and S. Turek, *FEM multigrid techniques for fluidstructure interaction with application to hemodynamics*, Appl. Numer. Math., 62 (2012), pp. 1156–1170.

[62] Y. Saad, *A flexible inner-outer preconditioned GMRES algorithm*, SIAM J. Sci. Comput., 14 (1993), pp. 461–469.

[63] Y. Saad, *Iterative Methods for Sparse Linear Systems*, SIAM, Philadelphia, 2003.

[64] Y. Saad and M. H. Schultz, *GMRES: A generalized minimal residual algorithm for solving nonsymmetric linear systems*, SIAM J. Sci. Stat. Comput., 7 (1986), pp. 856–869.

[65] M. Sala and R. Tuminaro, *A new Petrov-Galerkin smoothed aggregation preconditioner for nonsymmetric linear systems*, SIAM J. Sci. Comput., 31 (2008), pp. 143–166.

[66] J. Schöberl, *NETGEN-An advancing front 2D/3D-mesh generator based on abstract rules*, Comput. Visual. Sci., 1 (1997), pp. 41–52.

[67] J. Sokolowski and J. P. Zolesio, *Introduction to Shape Optimization*, Springer, Heidelberg, 1992.

[68] K. Takizawa, H. Takagi, T. Tezduyar, and R. Torii, *Estimation of element-based zero-stress state for arterial FSI computations*, Comput. Mech., (2013), pp. 1–16.

[69] R. Torii, M. Oshima, T. Kobayashi, K. Takagi, and T. Tezduyar, *Fluid-structure interaction modeling of a patient-specific cerebral aneurysm: influence of structural modeling*, Comput. Mech., 43 (2008), pp. 151–159.

[70] A. Toselli and O. Widlund, *Domain Decomposition Methods-Algorithms and Theory*, Springer, Heidelberg, 2005.

[71] S. Vanka, *Block-implicit multigrid solution of Navier-Stokes equations in primitive variables*, J. Comput. Phys., 65 (1986), pp. 138–158.

[72] P. Vassilevski, *Multilevel Block Factorization Preconditioners*, Springer, Heidelberg, 2008.

[73] M. Wabro, *Coupled algebraic multigrid methods for the Oseen problem*, Comput. Visual. Sci., 7 (2004), pp. 141–151.

[74] ——, *AMGe—coarsening strategies and application to the Oseen equations*, SIAM J. Sci. Comput., 27 (2006), pp. 2077–2097.

[75] T. Wick, *Fluid-structure interactions using different mesh motion techniques*, Comput. Structures, 89 (2011), pp. 1456–1467.
[76] H. Wobker and S. Turek, *Numerical studies of Vanka-type smoothers in computational solid mechanics*, Adv. Appl. Math. Mech., 1 (2009), pp. 29–55.
[77] H. Yang, *Numerical Simulation of Fluid-Structure Interaction Problems on Hybrid Meshes with Algebraic Multigrid Methods*, PhD thesis, Johannes Kepler University Linz, 2010.
[78] ——, *Partitioned solvers for the fluid-structure interaction problems with a nearly incompressible elasticity model*, Comput. Visual. Sci., 14 (2011), pp. 227–247.
[79] H. Yang and W. Zulehner, *Numerical simulation of fluid-structure interaction problems on hybrid meshes with algebraic multigrid methods*, J. Comput. Appl. Math., 235 (2011), pp. 5367–5379.
[80] W. Zulehner, *A class of smoothers for saddle point problems*, Computing, 65 (2000), pp. 227–246.

Johann Radon Institute for Computational and Applied Mathematics (RICAM), Austrian Academy of Sciences, Altenberger Strasse 69, A-4040 Linz, Austria
E-mail address: ulrich.langer@ricam.oeaw.ac.at
URL: http://www.ricam.oeaw.ac.at/people/u.langer/

Johann Radon Institute for Computational and Applied Mathematics (RICAM), Austrian Academy of Sciences, Altenberger Strasse 69, A-4040 Linz, Austria
E-mail address: huidong.yang@oeaw.ac.at
URL: http://people.ricam.oeaw.ac.at/h.yang/